Vol. 6 (2013) *Acta Physica Polonica B Proceedings Supplement* No 2

RECENT RESULTS FROM THE LHCf EXPERIMENT*

Gaku Mitsuka

on behalf of the LHCf Collaboration

Solar Terrestrial Environment Laboratory, Nagoya University
Nagoya, Aichi 464-8601, Japan

(Received January 25, 2013)

The Large Hadron Collider forward experiment measured very forward neutral particle spectra in LHC proton–proton collisions in early 2010. In this paper, we will discuss the transverse momentum spectra of neutral pion at the 7 TeV proton–proton collision and the inclusive photon energy spectra at the 900 GeV proton–proton collisions. The spectra in both collision energies are also compared with the predictions of several hadronic interaction models that are often used for high energy particle physics and for modeling ultrahigh-energy cosmic ray showers.

DOI:10.5506/APhysPolBSupp.6.599
PACS numbers: 13.85.Tp, 13.85.–t

1. Introduction

The Large Hadron Collider forward (LHCf) experiment [1] has been designed to measure the hadronic production cross sections of neutral particles emitted in very forward angles in proton–proton collisions at the LHC, including zero degrees. The LHCf detectors have the capability for precise measurements of forward high-energy inclusive-particle-production cross sections of photons, neutrons, and possibly other neutral mesons and baryons. The analyses in this paper concentrate on obtaining (1) the inclusive production rate for π^0s in the rapidity range larger than $y = 8.9$ as a function of the π^0 transverse momentum, and (2) the inclusive production rate for photons in the rapidity ranges $\eta > 8.77$ at 900 GeV as a function of the photon energy.

This work is motivated by an application to the understanding of ultra-high-energy cosmic ray (UHECR) phenomena, which are sensitive to the details of soft π^0 and photon production at extreme energy. It is known that the lack of knowledge about forward particle production in hadronic

* Presented at the International Symposium on Multiparticle Dynamics, Kielce, Poland, September 17–21, 2012.

collisions hinders the interpretation of observations of UHECR [2, 3]. Although UHECR observations have made notable advances in the last few years [4–8], critical parts of the analysis depend on Monte Carlo (MC) simulations of air shower development that are sensitive to the choice of the hadronic interaction model.

This paper is organized as follows. In Sec. 2, the LHCf detectors are described. The analyses results are then presented in Sec. 3 and Sec. 4. Finally, concluding remarks are found in Sec. 5.

2. The LHCf detectors

Two independent LHCf detectors, called Arm1 and Arm2, have been installed in the instrumentation slots of the target neutral absorbers (TANs) [9] located ± 140 m from the ATLAS interaction point (IP1) and at zero degree collision angle. Inside a TAN the beam-vacuum-chamber makes a Y-shaped transition from a single common beam tube facing IP1 to two separate beam tubes joining to the arcs of the LHC. Charged particles produced at IP1 and directed towards the TAN are swept aside by the inner beam separation dipole magnet D1 before reaching the TAN. Consequently, only neutral particles produced at IP1 enter the LHCf detector. At this location, the LHCf detectors cover the pseudorapidity range from 8.7 to infinity for zero degree beam crossing angle. With a maximum beam crossing angle of 140 μrad, the pseudorapidity range can be extended to 8.4 to infinity.

Each LHCf detector has two sampling and imaging calorimeters composed of 44 radiation lengths (X_0) of tungsten and 16 sampling layers of 3 mm thick plastic scintillator. The transverse sizes of the calorimeters are $20 \times 20\,\mathrm{mm}^2$ and $40 \times 40\,\mathrm{mm}^2$ in Arm1, and $25 \times 25\,\mathrm{mm}^2$ and $32 \times 32\,\mathrm{mm}^2$ in Arm2. The smaller and larger calorimeters are called as "small tower" and "large tower", respectively. The small towers cover zero degree collision angle. Four X–Y layers of position sensitive detectors are interleaved with the layers of tungsten and scintillator in order to provide the transverse positions of the showers. Scintillating fiber (SciFi) belts are used for the Arm1 position sensitive layers and silicon micro-strip sensors are used for Arm2. Readout pitches are 1 mm and 0.16 mm for Arm1 and Arm2, respectively.

3. Results of π^0 analysis at $\sqrt{s} = 7$ TeV

The combined p_T spectra of the Arm1 and Arm2 detectors are presented in Fig. 1 for six ranges of rapidity y: 8.9 to 9.0, 9.0 to 9.2, 9.2 to 9.4, 9.4 to 9.6, 9.6 to 10.0, and 10.0 to 11.0. The spectra in Fig. 1 are after all corrections for the detection inefficiency have been applied. The inclusive production rate of neutral pions is given by the expression

$$\frac{1}{\sigma_{\mathrm{inel}}} E \frac{d^3\sigma}{dp^3} = \frac{1}{N_{\mathrm{inel}}} \frac{d^2N(p_{\mathrm{T}}, y)}{2\pi\, p_{\mathrm{T}}\, dp_{\mathrm{T}}\, dy} \,. \tag{1}$$

σ_{inel} is the inelastic cross section for proton–proton collisions at $\sqrt{s} = 7\,\mathrm{TeV}$. $Ed^3\sigma/dp^3$ is the inclusive cross section of π^0 production. The number of inelastic collisions, N_{inel}, used for normalizing the production rates of Fig. 1 has been calculated from $N_{\mathrm{inel}} = \sigma_{\mathrm{inel}} \int \mathcal{L}dt$, assuming the inelastic cross section $\sigma_{\mathrm{inel}} = 73.6\,\mathrm{mb}$. This value for σ_{inel} has been derived from the best COMPETE fits [11] and the TOTEM result for the elastic scattering cross section [12]. Using the integrated luminosities reported in Ref. [10], N_{inel} is 1.85×10^8 for Arm1 and 1.40×10^8 for Arm2. $d^2N(p_{\mathrm{T}}, y)$ is the number of π^0s detected in the transverse momentum interval (dp_{T}) and the rapidity interval (dy) with all corrections applied. In Fig. 1, the 68 % confidence intervals incorporating the statistical and systematic uncertainties are indicated by the shaded green rectangles.

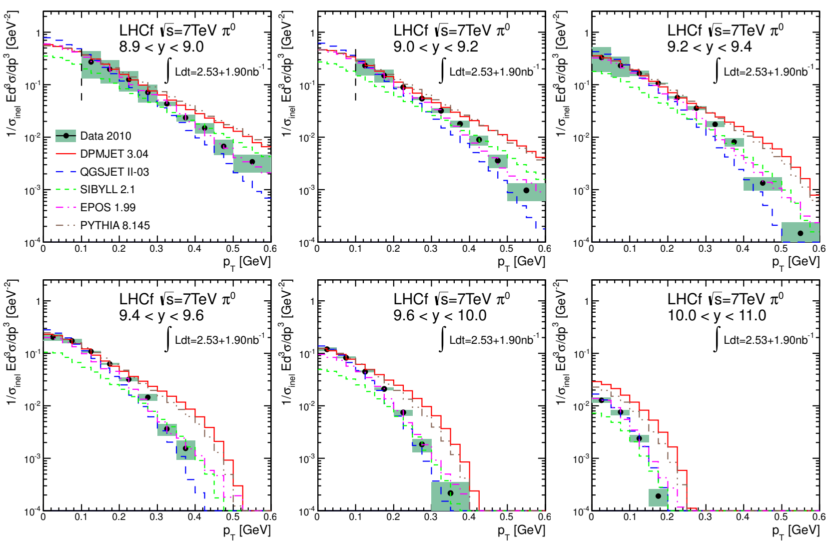

Fig. 1. Combined p_{T} spectra of the Arm1 and Arm2 detectors (black dots) and the total uncertainties (shaded rectangles) compared with the predicted spectra by hadronic interaction models.

For comparison, the p_{T} spectra predicted by various hadronic interaction models are also shown in Fig. 1. The hadronic interaction models that have been used in Fig. 1 are DPMJET 3.04 [13] (solid, red), QGSJET II-03 [14] (dashed, blue), SIBYLL 2.1 [15] (dotted, green), EPOS 1.99 [16] (dash-dotted, magenta), and PYTHIA 8.145 [17, 18] (default parameter set, dash-double-dotted, brown). In these MC simulations, π^0s from short lived particles that decay within 1 m from IP1, for example $\eta \to 3\pi^0$, are also counted to be consistent with the treatment of the experimental data. Note that, since the experimental p_T spectra have been corrected for the influences of the detector responses, event selection efficiencies and geometrical acceptance efficiencies, the p_T spectra of the interaction models may be compared directly to the experimental spectra as presented in Fig. 1.

Among hadronic interaction models tested in this analysis, Epos 1.99 shows the best overall agreement with the LHCf data. However, Epos 1.99 behaves softer than the data in the low p_T region, $p_T \lesssim 0.4\,\mathrm{GeV}$ in $9.0 < y < 9.4$ and $p_T \lesssim 0.3\,\mathrm{GeV}$ in $9.4 < y < 9.6$, and behaves harder in the large p_T region. Specifically, a dip found in the ratio of Epos 1.99 to the LHCf data for $y > 9.0$ can be attributed to the transition between two pion production mechanisms: string fragmentation via cut Pomeron process (low energy $\sim$ low p_T for the fixed rapidity) and remnants of projectile/target (high energy $\sim$ large p_T for the fixed rapidity).

4. Results of photon analysis at $\sqrt{s} = 900\,\mathrm{GeV}$

To reduce a possible pseudorapidity η dependence when comparing and combining the energy spectra measured by the two Arms, we selected Arm2 events with a pseudorapidity range similar to that of Arm1. For the small tower, we selected events with the distance r from the beam center less than 11 mm, which corresponded to the pseudorapidity range of $\eta > 10.15$

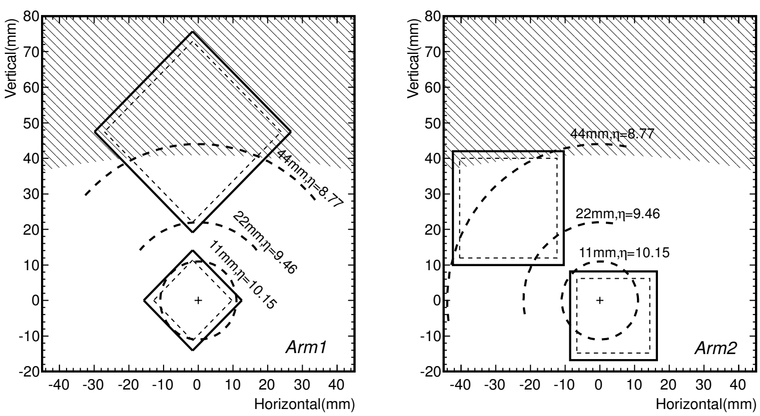

Fig. 2. The cross-sections of the calorimeters viewed from IP1, left for Arm1 and right for Arm2. The cross marks on the small calorimeters indicate the projections of the zero-degree collision angle onto the detectors ("beam center"). The shaded areas in the upper parts of the figure indicate the shadows of the beam pipes located between IP1 and the detectors, where the detectors are insensitive to the detection of IP1 proton–proton collision products. The dashed squares indicate the border of a fiducial area.

(the circles in Fig. 2). Similarly, for the large tower, we set the conditions as 22 mm $< r <$ 44 mm, which corresponded to the pseudorapidity range of $8.77 < \eta < 9.46$ (the arcs in Fig. 2). The calorimeters did not uniformly cover the pseudorapidity ranges as shown in Fig. 2. We confirmed that there was a negligible pseudorapidity dependence of the energy spectra inside each pseudorapidity range.

The combined energy spectra of Arm1 and Arm2 are shown in Fig. 3 as weighted averages, with the weights taken to be the square of the inverse of the errors in each energy bin. The error bars of the data (black points) represent the statistical error; the hatches in the spectra represent the total uncertainty (quadratical summation of the statistical and the systematic errors). The sources of the systematic error are the particle identification and the beam position uncertainties. The energy scale errors were also included, assuming a correlation between the two Arms. Note that the uncertainty of the luminosity determination ($\pm 21\,\%$) is not shown in Fig. 3. It can introduce a constant vertical shift of the spectra, but it cannot change the shapes of the spectra.

In Fig. 3, the predictions of the hadronic interaction models, QGSJET II-03, PYTHIA 8.145, SIBYLL 2.1, EPOS 1.99 and DPMJET 3.04, are also shown. The same analysis processes were applied to the MC simulations as to the experimental data except for the particle identification and its correction. For the analysis of the MC simulations, the known particle type was used. For better visibility, only the statistical errors for DPMJET 3.04 (red points) are shown by the error bars.

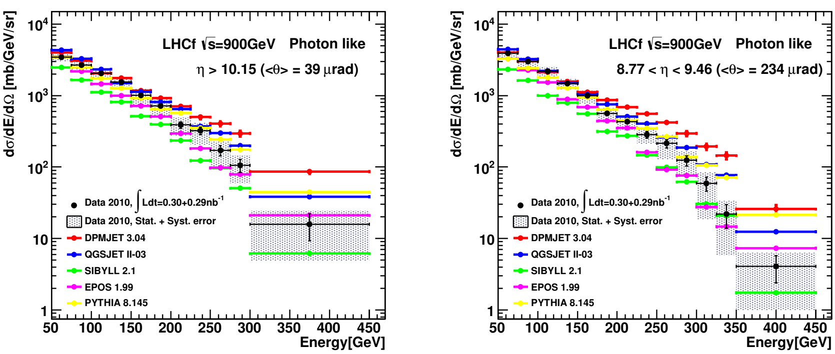

Fig. 3. Combined Arm1 and Arm2 photon energy spectra compared with MC predictions. The left and the right panels are the results of the small and the large towers, respectively.

5. Conclusions

The inclusive production of neutral pions in the rapidity range larger than $y = 8.9$ at $\sqrt{s} = 7$ TeV proton–proton collisions and the forward inclusive photon energy spectra in the pseudorapidity ranges of $\eta > 10.15$ and

$8.77 < \eta < 9.46$ for $\sqrt{s} = 900\,\mathrm{GeV}$ proton–proton collisions have been measured by the LHCf experiment in early 2010. Transverse momentum spectra of neutral pions and energy spectra of photons have been measured by two independent LHCf detectors, Arm1 and Arm2, and give consistent results.

The combined Arm1 and Arm2 spectra have been compared with the predictions of five hadronic interaction models, Dpmjet 3.04, Epos 1.99, Pythia 8.145, Qgsjet II-03 and Sibyll 2.1. For the neutral pion spectra, Dpmjet 3.04, Epos 1.99 and Pythia 8.145 agree with the LHCf combined results, in general, for the rapidity range $9.0 < y < 9.6$ and $p_{\mathrm{T}} < 0.2\,\mathrm{GeV}$. Qgsjet II-03 has poor agreement with LHCf data for $8.9 < y < 9.4$, while it agrees with LHCf data for $y > 9.4$. Among the hadronic interaction models tested in this paper, Epos 1.99 shows the best overall agreement with the LHCf data even for $y > 9.6$. For the photon spectra, Epos 1.99 and Sibyll 2.1 reproduce well the shape of the experimental energy spectra, but they predict a lower cross section than the LHCf data. The other models predict harder spectra than the LHCf data above 300 GeV. These results of comparison exhibited features similar to those for the previously reported data for $\sqrt{s} = 7\,\mathrm{TeV}$ collisions.

REFERENCES

[1] LHCf Technical Design Report, CERN-LHCC-2006-004.

[2] R. Ulrich, R. Engel, M. Unger, *Phys. Rev.* **D83**, 054026 (2011).

[3] R.D. Parsonsa, C. Bleveb, S.S. Ostapchenko, J. Knappa, *Astropart. Phys.* **34**, 832 (2011).

[4] J. Abraham *et al.*, *Phys. Rev. Lett.* **101**, 061101 (2008).

[5] J. Abraham *et al.*, *Phys. Rev. Lett.* **104**, 091101 (2010).

[6] R.U. Abbasi *et al.*, *Astropart. Phys.* **32**, 53 (2009).

[7] R.U. Abbasi *et al.*, *Phys. Rev. Lett.* **104**, 161101 (2010).

[8] H. Sagawa, *AIPC* **1367**, 17 (2011).

[9] W.C. Turner, E.H. Hoyer, N.V. Mokhov, Proc. of EPAC98, Stockholm, 1998, p. 368; LBNL Rep. LBNL-41964, 1998.

[10] O. Adriani *et al.*, *Phys. Lett.* **B703**, 128 (2011).

[11] K. Nakamura *et al.* [Particle Data Group], *J. Phys. G* **37**, 075021 (2010).

[12] G. Antchev *et al.* [TOTEM Coll.], *Europhys. Lett.* **96**, 21002 (2011).

[13] F.W. Bopp, J. Ranft, R. Engel, S. Roesler, *Phys. Rev.* **C77**, 014904 (2008).

[14] S. Ostapchenko, *Nucl. Phys. Proc. Suppl.* **151**, 143 (2006).

[15] E.-J. Ahn *et al.*, *Phys. Rev.* **D80**, 094003 (2009).

[16] K. Werner, F.-M. Liu, T. Pierog, *Phys. Rev.* **C74**, 044902 (2006).

[17] T. Sjöstand, S. Mrenna, P. Skands, *J. High Energy Phys.* **05**, 026 (2006).

[18] T. Sjöstand, S. Mrenna, P. Skands, *Comput. Phys. Commun.* **178**, 852 (2008).